Ultrafast tracking of second-order photon correlations in the emission of quantum-dot microresonator lasers

Marc Aßmann, Franziska Veit, and Manfred Bayer

Experimentelle Physik 2, Technische Universität Dortmund, 44221 Dortmund, Germany

Christopher Gies and Frank Jahnke

Institute for Theoretical Physics, University of Bremen, P.O. Box 330 440, 28334 Bremen, Germany

Stephan Reitzenstein, Sven Höfling, Lukas Worschech, and Alfred Forchel

Technische Physik, Physikalisches Institut, Wilhelm Conrad Röntgen Research Center for Complex Material Systems, Universität Würzburg, D-97074 Würzburg, Germany

Ultrafast changes in the statistical properties of light emission are studied for quantum-dot micropillar lasers. Using pulsed excitation with varying power, we follow the time evolution of the second-order correlation function $g^{(2)}(t, \tau=0)$ reflecting two-photon coincidences and compare it to that of the output intensity. The previously impossible time resolution of a few picoseconds gives insight into the dynamical transition between thermal and coherent light emission. The $g^{(2)}$ results allow us to isolate the spontaneous and stimulated-emission contributions within an emission pulse, not accessible via the emission-intensity dynamics. Results of a microscopic theory confirm the experimental findings.

Miniaturization of lasers currently attracts considerable interest, as the combination of tailoring the electronic states in quantum structures and engineering the light field in a resonator allows for the realization of light sources with high power-conversion efficiency. The standard tool for characterizing laser structures is the input-output curve, which measures the emission intensity versus optical or electrical pumping power. In conventional devices, the onset of lasing is identified as a jump in the input-output curve. Insight into the light-emission dynamics can be taken from time-resolved photoluminescence experiments. Both methodologies give, however, only limited insight into the buildup of coherence in an emission pulse from the laser.

Recent progress in experimental techniques has allowed us to access the second-order photon-correlation function,

$$g^{(2)}(t,\tau) = \frac{\langle \hat{b}^\dagger(t)\hat{b}^\dagger(t+\tau)\hat{b}(t+\tau)\hat{b}(t)\rangle}{\langle \hat{b}^\dagger(t)\hat{b}(t)\rangle\langle \hat{b}^\dagger(t+\tau)\hat{b}(t+\tau)\rangle} \qquad (1)$$

as a tool to gather information about the statistical properties of light sources.[1,2] Here $\hat{b}^\dagger$ and $\hat{b}$ are the photon creation and annihilation operators for the considered optical mode. $g^{(2)}(t, \tau)$ is determined by the joint probability for subsequent emission events of two photons with a relative time delay of τ. For spontaneous emission, such an interdependence is expected in the form of photon bunching as long as τ does not exceed the coherence time while for stimulated emission, the interdependence vanishes, no matter what delay is considered. Correspondingly, the equal-time correlation function $g^{(2)}(t, 0)$ is expected to take values of 2 and 1 in the regime of thermal and coherent emission, respectively. However, up to now studies of semiconductor lasers were hampered by the limited time resolution in the nanosecond range of Hanbury Brown–Twiss setups[3] used for measuring the

second-order correlation.[4,5] In particular, such experiments cannot provide insight into the dynamical evolution of this interdependence. Under pulsed excitation, the limited time resolution allows only for measurements of $g^{(2)}(\tau)$ averaged over all times t inside a pulse duration, with τ being an integer multiple of the delay time between two pulses.

While being suitable for any laser, we apply the technique here to a system of particular current interest, namely, quantum-dot (QD) microcavity lasers.[6] Superior performance compared to higher-dimensional systems has been predicted for them, such as a reduction in the laser threshold or increased temperature stability.[7–10] When miniaturized, however, the sharp transition from spontaneous to stimulated emission in the input-output curve is no longer present in these systems that are affected by quantum-electrodynamic effects.[11–13] Further, for excitation by short light pulses, QD lasers show saturation effects, leading to a reduction in the jump in the input-output curve.[14] These features make the study of the coherence dynamics within an emission pulse, which so far has been impossible also for other semiconductor lasers, particularly appealing for QD lasers.

In the following, measurements of the time-resolved photon-correlation properties of QD micropillar lasers under pulsed excitation are presented. We examine the buildup and breakdown of second-order coherence during the emission pulse by measuring the equal-time correlation function $g^{(2)}(t,0)$ at various times inside the pulse for different excitation densities around the lasing threshold. The measurements are compared to the results of a microscopic theory for the QD laser system.

The studied microresonator with a diameter of 6 μm is composed of two Bragg mirrors consisting of 20 upper and 23 lower alternating layers of alternating AlAs (79 nm)-GaAs (67 nm) $\lambda/4$ pairs surrounding a λ cavity containing a single layer of self-assembled (In,Ga)As QDs with a density
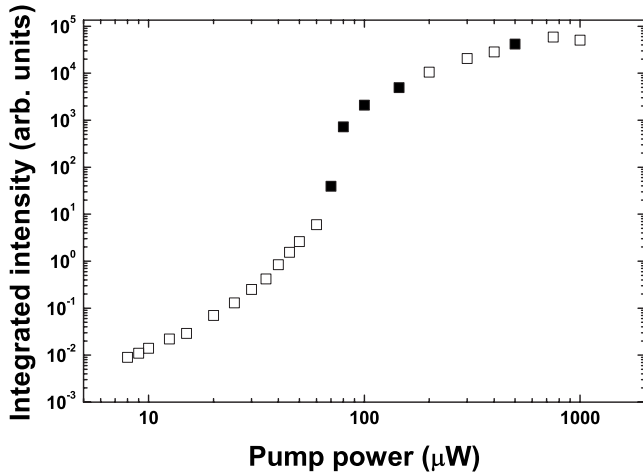
FIG. 1. Integrated intensity of the 6 μm pillar's fundamental mode under nonresonant pulsed excitation. Above threshold, saturation effects become apparent. Filled squares mark the data sets shown in Fig. 2.

of $\approx 3 \times 10^{10}$ cm^{-2} in the center. The sample was inserted in a helium-flow cryostat and cooled to a temperature of 10 K. For optical excitation, we used a pulsed Ti-Sapphire laser, emitting picosecond-light pulses with a wavelength of 780 nm at a rate of 75.39 MHz. The emission was focused onto a single micropillar by a microscope objective with a numerical aperture of 0.26, which was also used for collecting the micropillar emission. The spot had a diameter of approximately 10 μm, covering the whole pillar. Emitted light at a particular wavelength was selected by an interference filter with a 1-nm-wide transmission and directed into the streak camera, which provides a time resolution of 2 ps.

The key point of the experiment is the time-resolved recording of the individual photon emission events in the output pulse after each excitation, using a streak camera as described in Refs. 1 and 2. A large number of individually evaluated repetitions provides the statistical information about the dynamics of the intensity correlation function as well as the time evolution of the mean photon number. The method provides a complete mapping in t and τ of the second-order correlation function, Eq. (1), for the emitted light. Instead of determining the τ dependence by calculating the intensity-weighted average of $g^{(2)}(t,\tau)$ over a time interval t during the emission pulse, as done in Refs. 1 and 2, we consider here the t dependence at a fixed delay time of photon pairs $\tau = 0$. While the former gives a good characterization of the photon statistics and coherence time of the emitted pulse as a whole, the latter is a good measure of the time-resolved second-order coherence properties inside the pulse.

We identified the transition region to lasing of the micropillar by measuring the input-output curve shown in Fig. 1. A nonlinear behavior between excitation powers of 60 and 150 μW marks this region. At lower excitation powers, $g^{(2)}(t,0)$ takes on the expected static value of 2 without any dynamics. More interesting are the excitation powers (filled squares in Fig. 1) in and above the threshold region for which we determine the intensity-dependent second-order coherence properties of the emission.
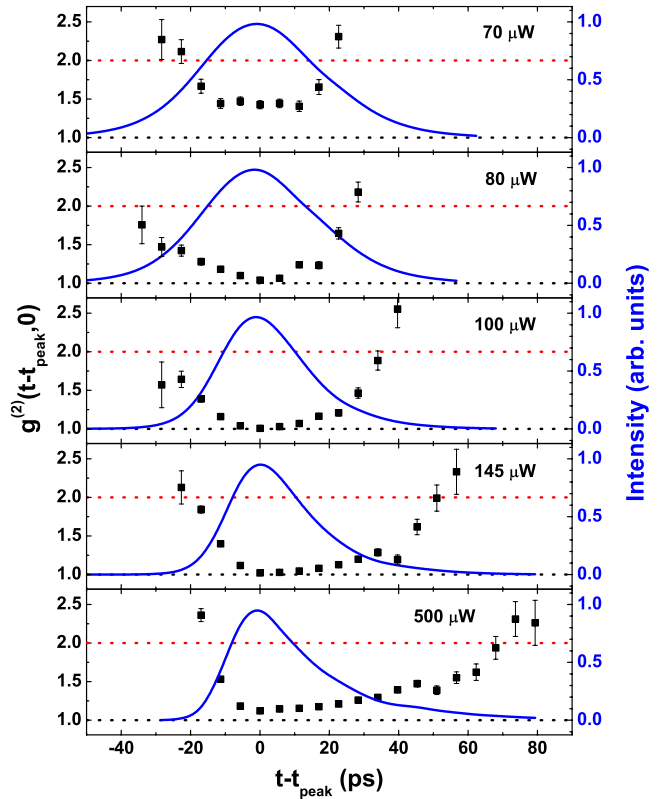

FIG. 2. (Color online) Time evolution of second-order photon-correlation function $g^{(2)}(t,0)$ (symbols) compared to the normalized output intensity (solid lines) for the 6 μm pillar fundamental mode. Black and red dotted lines denote the limiting cases of $g^{(2)}(t,0)$ for coherent and thermal light, respectively. The power density for pulsed excitation increases from top to bottom. t_{peak} corresponds to the maximum of the emission intensity for each pump power.

In Fig. 2, $g^{(2)}(t,0)$ is shown for these excitation powers alongside the temporal emission-intensity profiles. The light exhibits thermal behavior at the very beginning and at the very end of the emission pulse. After the generation of carriers in the barrier states by the pump pulse, these carriers rapidly relax into the QD states.[15] As long as a small number of carriers is present in the QD states, spontaneous recombination processes determine the output. When the population becomes sufficiently strong, the system is driven into the regime of coherent emission, characterized by a decrease in the second-order correlation function toward the value of 1, and by a faster decay of the emission intensity due to the stimulated processes, visible in an apparent temporal narrowing of the emission peak. The decrease toward $g^{(2)}(0) = 1$ becomes more pronounced for higher excitation densities, finally leading to a broadening of the dip, as more carriers are excited in the system and stimulated emission can be maintained for a longer time. While the transition from thermal to coherent emission in the beginning of the pulsed emission can take 40 ps or even more in the threshold region, it happens on a time scale on the order of 10–15 ps far above threshold.

As another important finding, it should also be noted that knowledge of $g^{(2)}$ allows us to determine how large the relative amounts of coherent and thermal emission are for any
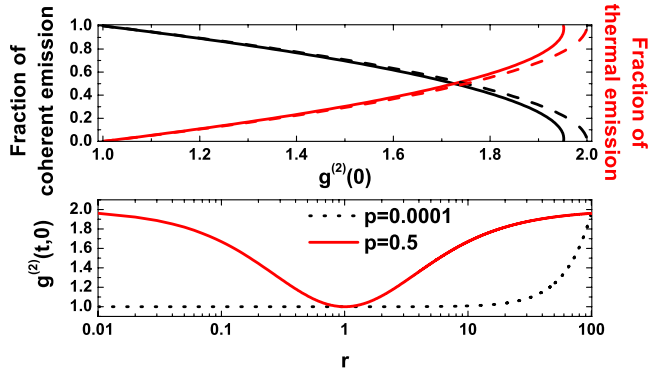
FIG. 3. (Color online) Upper panel: relative fractions of coherent and thermal emission at a fixed $g^{(2)}(t,0)$ as given by a two-mode model (solid lines) compared to the ideal case for infinitely small sampling time (dashed lines). Small deviations occur at high thermal fractions. Lower panel: effect of jitter on the measured $g^{(2)}(t,0)$ for a coherent light pulse depending on the ratio r of the mean photon count rates at the pulse positions connected by the jitter and the relative frequency p of jitter occurrence. While frequent jitter (solid red line) has the same effects for pulse positions with high and low intensity, rare events (dotted black line) only affect regions with low mean photon count rate (high r).

given time within the emission pulse. This information is not accessible via output intensity measurements alone. One can consider partially coherent light as a superposition of a thermal and a coherent mode, which contribute to $g^{(2)}$ according to[16]

$$g^{(2)}(t,0) = \left(1 + \frac{1}{\gamma} - \frac{1}{2\gamma^2} + \frac{e^{-2\gamma}}{2\gamma^2}\right)R_t^2$$
$$+ g_c^{(2)}(t,0)R_c^2 + 2R_t R_c\left(1 + \frac{2e^{-\gamma}}{\gamma^2} + \frac{2}{\gamma} - \frac{2}{\gamma^2}\right),$$
(2)

where $\gamma = \Gamma T$ with $h\Gamma \approx 63$ μeV is the thermal mode half width at half maximum and $T = 5$ ps is the sampling time. As can be seen in Fig. 3, the thermal and coherent fractions depend nonlinearly on $g^{(2)}$ showing that already small amounts of thermal emission can cause significant deviations from coherent emission. The finite sampling time causes a slight underestimation of $g^{(2)}$ for large thermal fractions. In our case, the minimum $g^{(2)}$ for 70 μW excitation power is about 1.5, for which about 70% of the emission is coherent. When $g^{(2)}$ drops on the other hand below 1.2, more than 90% of the emitted light is coherent.

We note that in the time evolution of the second-order coherence $g^{(2)}(t,0)$, the position of the minimum coincides with the peak of the mean photon number of the emission pulse. Also the time dependence of the leading and trailing edges of the emission pulse is mirrored in the dynamics of $g^{(2)}(t,0)$. This suggests that the interplay of stimulated emission and output coupling determines not only the emission intensity but also the coherence properties. This behavior appears surprising as the dynamical evolution of the mean photon number $\langle \hat{b}^\dagger(t)\hat{b}(t)\rangle$ and of the two-photon coinci-

dences $\langle \hat{b}^\dagger(t)\hat{b}^\dagger(t)\hat{b}(t)\hat{b}(t)\rangle$ obey distinctly different equations of motion in which different types of carrier-photon correlations enter (see, e.g., Ref. 17), even though both expectation values can be traced back to the time dependence of the photon probability distribution.

At the very early and late parts of the emission pulse, where low values of the emitted intensity are present, an overshoot of $g^{(2)}(t,0)$ beyond the thermal value of 2 is obtained in the experiment.[18] This behavior is an artifact of pulse jitter caused by electronic noise. The normalized $g^{(2)}(t,0)$ is the mean photon pair count rate at a screen position corresponding to time t normalized by the squared mean photon count rate at the same position. However, due to jitter of the excitation source or electronic jitter of the trigger signal, the signal pulse does not always appear on exactly the same position but the peak position varies following a Gaussian distribution with a standard deviation of approximately 1.5 ps. Therefore, the detected mean photon pair and photon count rates at a screen position corresponding to time t are in fact a mixture of all photon pair and photon count rates weighted with a narrow Gaussian distribution centered at t. To determine whether this jitter has a significant effect on the recorded photon statistics, it is necessary to compare the time scale on which the jitter occurs to the time scale of the pulse dynamics. If the pulse dynamics are comparable to the jitter time scale or even faster, the momentary intensity at a certain position on the screen will vary strongly from picture to picture and the measured correlation function will depend on these fluctuations instead of the intrinsic fluctuations of the light field. For visualization of this effect, let us consider a coherent pulse with varying intensity and a simplified jitter, which leads to well defined shift Δt with a probability p and causes no shift at all other times with the probability $q = 1 - p$. The measured intensity correlation at a position on the screen corresponding to time t will now only depend on p and the mean photon number ratio $r = \frac{n(t+\Delta t)}{n(t)}$ of the times connected by the jitter,

$$g^{(2)}(t,0) = \frac{qn(t)^2 + p[rn(t)]^2}{[qn(t) + prn(t)]^2} = \frac{q + pr^2}{(q + pr)^2}.$$
(3)

This function is depicted in the lower part of Fig. 3 for rare events (black dotted line) and common events (red solid line). The detrimental effect of the common jitter shown there is negligible for our measurement because common jitter happens on a time scale of about 1.5 ps and the mean photon count rates do not change significantly in this range. Even at the steepest positions of the pulse slope, the intensity variation does not exceed 7% within 1.5 ps (cf. Fig. 2). Accordingly, only the region between $r = 0.93$ and $r = 1.07$, where the red line does not show significant deviations from the expected value of 1, contributes for frequent jitter. For rare events on the other hand, there is no effect for small r but there are significant deviations for $r \gtrsim 20$. As Gaussian jitter is unbounded, there are indeed rare jitter events where r exceeds 20 for regions with small mean photon count rate. These rare events cause the overshoot of $g^{(2)}(t,0)$ seen far from the emission peak in Fig. 2. In these regions, the increased pair detection rate due to rare jitter events is larger

than the intrinsic photon pair count rate determined by the mean intensity at this position. For Gaussian jitter, the real and the jitter-induced $g^{(2)}$ add quadratically. This consideration shows that special care must be exercised when the statistics of weak emission signals are studied.

We compare the experimental findings to results of a microscopic theory, that has been developed recently to describe the emission properties of semiconductor microcavity lasers with QDs as active material.[17] The theory is based on equations of motions for the mean photon number and the QD carrier occupation probabilities, that generalize the so-called semiconductor luminescence equations.[19,20] We consider the coupling to a set of higher-order expectation values, including carrier-photon correlations as well as higher-order photon expectation values that describe $g^{(2)}(t, \tau = 0)$. The hierarchy of equations is decoupled using the cluster-expansion technique as described in Ref. 17.

The experimental situation includes excitation into barrier states and subsequent carrier relaxation and capture into QD states, determined by the carrier-carrier Coulomb interaction and carrier-phonon interaction.[21–24] Since the details of these processes are not crucial for the photon-correlation dynamics, the following simplified model is used for the carrier excitation. We consider QDs with ground and excited states, as in Ref. 17, and assume incoherent generation of carriers in the excited QD states with a time-dependent rate determined by an effective pump pulse. The model includes subsequent carrier relaxation into the lowest QD states that are coupled to the fundamental cavity mode. Carrier scattering and dephasing rates are obtained from independent many-body calculations. A pulse duration of 68 ps provides a reasonable estimate for the population dynamics of the excited QD states to obtain an evolution of the output intensity as observed in the experiment. This value is in reasonable accord with recent studies on similar QD structures, which give luminescence rise times on the order of 50 ps.[15]

The calculated time-resolved intensity and second-order correlation function $g^{(2)}(t, \tau = 0)$ are shown in Fig. 4. For increasing values of the time-integrated pump rate from $P = 3$ to $P = 7$, we find the temporal narrowing of the output pulse due to the increasing stimulated-emission contribution accompanied by a growing dip in the photon-correlation function approaching unity at the intensity maximum. With increasing pump rate, inversion of the carrier states is reached earlier and persists longer. For the highest pump rate $P = 10$, saturation effects due to Pauli blocking start to reduce the
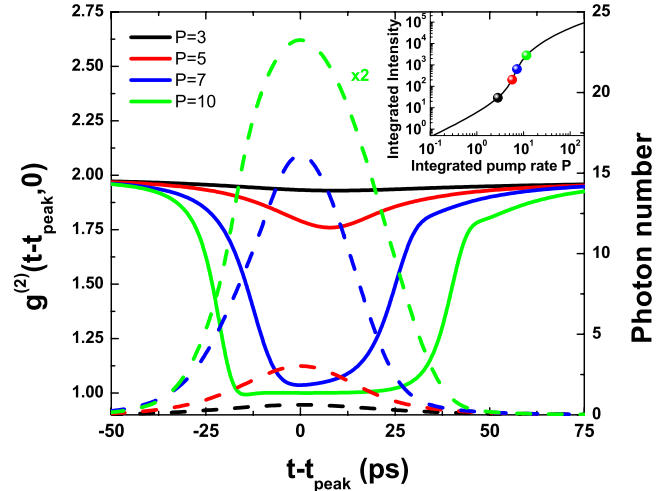

FIG. 4. (Color online) Calculated input-output curve (inset) and time evolution of the mean photon number (dashed lines) and the second-order correlation function (solid lines) for selected values of the time-integrated pump rate indicated by the color-coded dots on the input-output curve. All curves are calculated for a pump-pulse width of 68 ps. The following parameters were used: number of resonant QDs: 140, cavity loss rate $2 \kappa: 0.09 \ \mathrm{ps}^{-1}$, spontaneous lifetime: 4.3 ps, scattering rates into (out of) the lasing transition: 11.7 ps^{-1}(23.3 ps^{-1}), light-matter coupling constant $g: 0.22 \ \mathrm{ps}^{-1}$, loss rate to nonlasing modes: $\Gamma_{nl} = 0.22 \ \mathrm{ps}^{-1}$, and constant dephasing: $\Gamma = 8.5 \ \mathrm{ps}^{-1}$. Comparison with extended calculations including an inhomogeneously broadened ensemble gives very similar results with the present calculations using a homogeneous ensemble subject to considerable dephasing.

peak intensity of the output pulse. As a consequence, these saturation effects also lead to the appearance of a longer pulse duration (Fig. 4).

In summary, we have developed a technique, which allows us to experimentally address the dynamical evolution of equal-time intensity correlations under nonstationary conditions. While applied here to QD microcavity lasers, this technique is prospective for reaching a deeper stage of insight into arbitrary solid-state light sources.

[1] J. Wiersig, C. Gies, F. Jahnke, M. Aßmann, T. Berstermann, M. Bayer, C. Kistner, S. Reitzenstein, C. Schneider, S. Höfling, A. Forchel, C. Kruse, J. Kalden, and D. Hommel, Nature (London) **460**, 245 (2009).

[2] M. Aßmann, F. Veit, M. Bayer, M. van der Poel, and J. M. Hvam, Science **325**, 297 (2009).

[3] R. Hanbury Brown and R. Q. Twiss, Nature (London) **177**, 27 (1956).

[4] S. M. Ulrich, C. Gies, S. Ates, J. Wiersig, S. Reitzenstein, C. Hofmann, A. Löffler, A. Forchel, F. Jahnke, and P. Michler, Phys. Rev. Lett. **98**, 043906 (2007).

[5] S. Strauf, K. Hennessy, M. T. Rakher, Y.-S. Choi, A. Badolato, L. C. Andreani, E. L. Hu, P. M. Petroff, and D. Bouwmeester, Phys. Rev. Lett. **96**, 127404 (2006).

[6] K. J. Vahala, Nature (London) **424**, 839 (2003).

[7] Z. I. Alferov, Rev. Mod. Phys. **73**, 767 (2001).

[8] Z. G. Xie, S. Götzinger, W. Fang, H. Cao, and G. S. Solomon, Phys. Rev. Lett. **98**, 117401 (2007).

[9] S. Reitzenstein, C. Böckler, A. Bazhenov, A. Gorbunov, A. Löffler, M. Kamp, V. D. Kulakovskii, and A. Forchel, Opt. Express **16**, 4848 (2008).

[10] M. Nomura, N. Kumagai, S. Iwamoto, Y. Ota, and Y. Arakawa, Opt. Express **17**, 15975 (2009).

[11] P. R. Rice and H. J. Carmichael, Phys. Rev. A **50**, 4318 (1994).

[12] F. De Martini and G. R. Jacobovitz, Phys. Rev. Lett. **60**, 1711 (1988).

[13] Y. Yamamoto, S. Machida, and G. Björk, Phys. Rev. A **44**, 657 (1991).

[14] C. Gies, J. Wiersig, and F. Jahnke, Phys. Rev. Lett. **101**, 067401 (2008).

[15] H. Kurtze, J. Seebeck, P. Gartner, D. R. Yakovlev, D. Reuter, A. D. Wieck, M. Bayer, and F. Jahnke, Phys. Rev. B **80**, 235319 (2009).

[16] E. Jakeman and E. R. Pike, J. Phys. A **2**, 115 (1968).

[17] C. Gies, J. Wiersig, M. Lorke, and F. Jahnke, Phys. Rev. A **75**, 013803 (2007).

[18] Additional differences between the real and the measured $g^{(2)}$ can be caused by dark counts. The influence of dark counts is a question of the signal-to-noise ratio. A low signal-to-noise ratio usually decreases the measured value of $g^{(2)}$ below the real one. In fact, dark counts can approximately be treated as a superposed mode of uncorrelated detections without cross correlation to the signal. The deviation between measured and real $g^{(2)}$ is approximately 10% at a signal-to-noise ratio of 100/5 and 2% at a signal-to-noise ratio of 100/1. Accordingly, all of our experiments were performed with a signal-to-noise better than 100/1.

[19] N. Baer, C. Gies, J. Wiersig, and F. Jahnke, Eur. Phys. J. B **50**, 411 (2006).

[20] T. Feldtmann, L. Schneebeli, M. Kira, and S. W. Koch, Phys. Rev. B **73**, 155319 (2006).

[21] J. Urayama, T. B. Norris, J. Singh, and P. Bhattacharya, Phys. Rev. Lett. **86**, 4930 (2001).

[22] E. Péronne, F. Fossard, F. H. Julien, J. Brault, M. Gendry, B. Salem, G. Bremond, and A. Alexandrou, Phys. Rev. B **67**, 205329 (2003).

[23] F. Quochi, M. Dinu, L. N. Pfeiffer, K. W. West, C. Kerbage, R. S. Windeler, and B. J. Eggleton, Phys. Rev. B **67**, 235323 (2003).

[24] E. W. Bogaart, J. E. M. Haverkort, T. Mano, T. van Lippen, R. Nötzel, and J. H. Wolter, Phys. Rev. B **72**, 195301 (2005).